Journal of Molecular Graphics and Modelling 27 (2008) 88–94

Contents lists available at ScienceDirect

Journal of Molecular Graphics and Modelling

journal homepage: www.elsevier.com/locate/JMGM

Temperature-induced unfolding pathway of a type III antifreeze protein: Insight from molecular dynamics simulation

Sangeeta Kundu, Debjani Roy *

Bioinformatics Centre, Bose Institute, Kolkata, India

ARTICLE INFO

Article history:
Received 14 December 2007
Received in revised form 15 February 2008
Accepted 11 March 2008
Available online 16 March 2008

Keywords:
Antifreeze protein
Molecular dynamics
Principal component analysis
Unfolding
Transition state

ABSTRACT

Molecular dynamics simulations of the temperature-induced unfolding reaction of a cold-adapted type III antifreeze protein (AFPIII) from the Antarctic eelpout *Lycodichthys dearborni* have been carried out for 10 ns each at five different temperatures. While the overall character and order of events in the unfolding process are well conserved across temperatures, there are substantial differences in the timescales over which these events take place. Plots of backbone root mean square deviation (RMSD) against radius of gyration (Rg) serve as phase space trajectories. These plots also indicate that the protein unfolds without many detectable intermediates suggestive of two-state unfolding kinetics. The transition state structures are identified from essential dynamics, which utilizes a principal component analysis (PCA) on the atomic fluctuations throughout the simulation. Overall, the transition state resembles an expanded native state with the loss of the three 3_{10} helices and disrupted C-terminal region.

Our study provides insight into the structure–stability relationship of AFPIII, which may help to engineer AFPs with increased thermal stability that is more desirable than natural AFPs for some industrial and biomedical purposes.

1. Introduction

Many plants, insects, animals and other organisms have evolved with unique adaptive mechanisms that allow them to survive in harsh environment. Organisms that are adapted to extreme cold environment are often termed psychrophiles. A special class of cold-adapted proteins is the antifreeze proteins (AFPs). Some bacteria, fungi, plants invertebrates and vertebrates living in cold environments prevent cell or tissue damage from freezing by producing AFPs [1]. AFPs depress the freezing points of blood and body fluids below that of the surrounding seawater by binding to and inhibiting the growth of seed ice crystals [2]. AFPs have many potential applications, including their use as additives to improve the quality and shelf-life of frozen food, as cryoprotective agents for organ and cell cryopreservation, as chemical adjuvants to cancer cryosurgery and in the development of transgenic plants and animals with increased tolerance to cold [1,3–5]. For some uses, such as food processing, any added AFP may also need to withstand heat treatment (pasteurization). Unfortunately, the physiological temperatures of different AFPs appear to be low. This may facilitate unwanted degradation or irreversible aggregation, leading to inactivation during storage [6] and/or eventual heat treatment, such as pasteurization. Engineered AFPs with increased thermo stability may be more desirable than natural AFPs for some industrial and biomedical purposes. To date very limited molecular dynamics (MD) study dealing with thermo stability of AFPIII has been done. Because of their generally small size and relatively simple structure AFPIIIs may be ideally suited for molecular dynamics simulation which provides further insights into the conformational stability of cold-adapted proteins. In order to gain a deeper insight into the structural features responsible for thermo stability of the antifreeze protein we have employed molecular dynamics simulations on the available crystal structure of AFPIII from the Antarctic eel pout *Lycodichthys dearborni* [7] for 10 ns each at five different temperatures namely 277 K, 298 K, 373 K, 423 K and 473 K. Thus the starting structure of AFPIII (Fig. 1) for molecular dynamics simulation is comprised of 64 residues that folds into one α-helix (residues 37–40), three 3_{10} helices (residues 19–21, 34–36 and 57–59) and two β-strands (residues 4–7 and 22–25) similar to other AFPIIIs. The structure has seven additional β-bridges. The protein exhibits a flat ice-binding patch on its surface.

We investigated the structure–stability relationship with focus on possible differences in the thermal unfolding pathway. The unfolding process has been carefully monitored both at an overall and a detailed structural level. We have especially analyzed the structures to see if there are important molecular contacts, which could explain the observed difference in thermal stability of this

* Corresponding author at: Bioinformatics Centre, Bose Institute, Acharya J.C. Bose Centenary Building, P-1/12 C.I.T Scheme-VII M, Kolkata 700054, India. Tel.: +91 33 2355 6626/91 33 2355 2816; fax: +91 33 2334 3886.
E-mail address: debjani@bic.boseinst.ernet.in (D. Roy).

1093-3263/$ – see front matter © 2008 Published by Elsevier Inc.
doi:10.1016/j.jmgm.2008.03.002

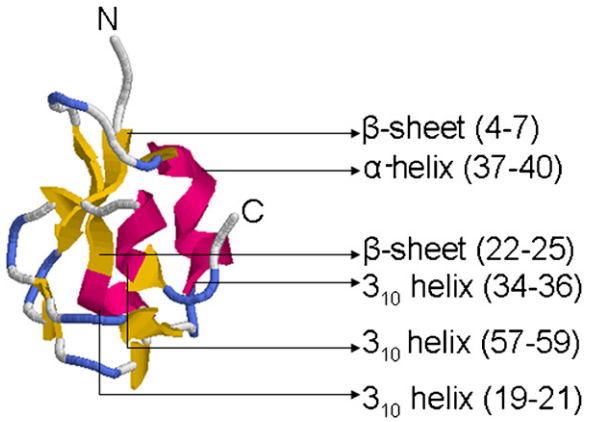

Fig. 1. The native structure of AFPIII (1UCS.pdb). Helices are shown as magenta ribbons, β-strands as yellow arrows and the rest are shown as loops.

protein as well as to identify the intermediate conformational states that the protein might visit during the unfolding process. Our study may help to engineer AFPs with increased thermal stability that is more desirable than natural AFPs for some industrial and biomedical purposes.

2. Methodology

2.1. Molecular dynamics simulation

Molecular dynamics simulations were performed using the GROMACS 3.3.1 [8,9] package and GROMOS96 [10] 43a1 force field implemented on LINUX architecture. 0.62-Å-resolution crystal structure of AFPIII protein from the Antarctic eel pout *L. dearborni* (PDB code: 1UCS) [7] was used as starting point for MD simulations. The protein was solvated in a triclinic 5.09 nm × 4.93 nm × 4.77 nm box of 3640 SPC [11] water molecules. No counter ions were added because the system was already neutral. All protein atoms were at a distance equal to 1.0 nm from the box edges. The system was subjected to energy minimization for 2000 steps by steepest descent. The minimized system was equilibrated for 50 ps each at five different temperatures (277 K, 298 K, 373 K, 423 K and 473 K) by position restrained molecular dynamics simulation in order to relax the solvent. The equilibrated systems were then subjected to molecular dynamics simulations for 10 ns each at five different temperatures. Periodic boundary conditions combined with minimum image convention were used under isothermal, isobaric conditions. Berendsen coupling [12] and LINCS algorithm [13] were used. The time step of the simulation was 2 fs. Electrostatic interactions were calculated using the Particle Mesh Ewald (PME) [14,15] summation scheme. van der Waals and coulomb interactions were truncated at 1.0 nm. The non-bonded pair list was updated every 10 steps and conformations were stored every 0.5 ps. Secondary structure analysis was performed using the program DSSP [16]. Other analyses were performed using scripts included with the Gromacs [17] distribution. The visual analysis of protein structures was carried out using Rasmol [18].

2.2. Potential energy contour map

In order to generate the three-dimensional potential energy contour map the backbone root mean square deviation (RMSD), radius of gyration (Rg), and potential energy of the system were plotted for all five simulations using ORIGIN program (version 6.0).

2.3. Calculation of principal components

The calculation of the eigenvectors and eigenvalues, and their projection along the first two principal components, was carried out using essential dynamics method according to protocol of Amadei et al. [19] within the GROMACS software package [17]. The essential dynamics method divides the conformational space of the protein into two subspaces, an essential subspace and a non-essential, physically constrained subspace. The first step of essential dynamics is the generation of non-mass weighted coordinate matrix. For an N atom system, this will be 3N × 3N matrix which is denoted as *A*. The covariance matrix of *A*, denoted as *C* is defined by the following equation:

$$C = A^{\mathrm{T}}A \tag{1}$$

where T is the transpose of the matrix. The transpose is obtained by exchanging the rows and columns of the matrix. The eigenvectors of the covariance matrix represent the principal components. This then appears into a simple eigenvalue problem:

$$Cx = \lambda x \tag{2}$$

where λ is the eigenvalue associated with the eigenvector *x*. For an N atom system, there are 3N eigenvectors and associated eigenvalues. Eq. (2) can be simplified to the following:

$$(C - \lambda I)x = 0 \tag{3}$$

where *I* is the identity matrix. The solution to Eq. (3) can be obtained by diagonalizing the covariance matrix. The diagonal matrix, *D*, of the covariance matrix is defined by the following:

$$D = U^{-1}CU \tag{4}$$

The matrix *U* contains the eigenvectors, and *D* is a matrix of the corresponding eigenvalues. The eigenvector with the highest eigenvalue is considered the first principal component; the eigenvector with the second highest eigenvalue is considered the second principal component and so on. The eigenvectors represent the direction of motion, and the eigenvalues represent the amount of motion along the eigenvectors. It has been suggested that the majority of the motion for proteins can be accounted for in the first two principal components. Therefore, the dynamics of a protein can be analyzed by projecting its atomic motion during a MD simulation onto its first two principal components. Essential dynamics is an efficient tool for monitoring protein dynamics in phase space because the observed motion is unconstrained and represents the atomic fluctuations of the protein.

3. Results and discussion

3.1. Analysis of the simulations

The major focus of this study is to compare the dynamic behaviors of this protein at 277 K, 298 K, 373 K, 423 K and 473 K. To that end we compare a range of features between the trajectories generated at five different temperatures. As the physiological temperature for antifreeze protein is close to 0 °C (273 K) the lowest temperature tested for MD simulation is 4 °C (277 K). From 4 °C (277 K) the temperature is gradually raised up to 200 °C (473 K) at which the protein is essentially denatured. Even higher temperatures are tested but the trajectories generated beyond 473 K yield complete loss of ordered structure within just a few ps. The resulting trajectories are too difficult to analyze as most of the sampling are on the fully folded poly-peptide chains.

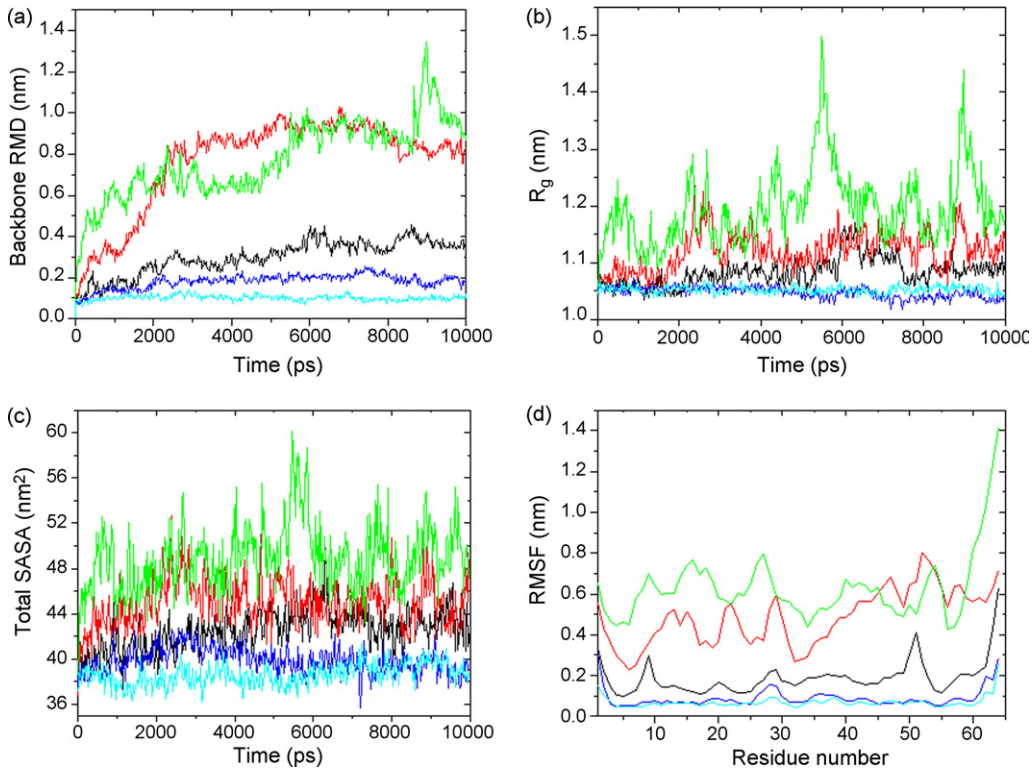

Fig. 2. Time evolution of (a) Backbone RMSD, (b) radius of gyration and (c) solvent accessible surface area of the protein at different temperatures. (d) The RMSFs of Cα coordinates are shown as a function of residue number at different temperatures. The color-coding scheme is as follows: 277 K (cyan), 298 K (blue), 373 K (black), 423 K (red) and 473 K (green).

3.1.1. RMSD

The RMSD of the backbone atoms of the protein from the starting structure over the course of simulation may be used as a measure of the conformational stability of a protein during that simulation. The plots of RMSD of the protein versus time at different temperatures are shown in Fig. 2a. The average RMSD is ~0.1 nm for the backbone atoms of the run at 277 K.

In the trajectory run at 298 K the backbone RMSD increases slightly from the starting conformation, which fluctuates, between 0.15 nm and 0.2 nm during the simulation.

In the trajectory run at 373 K RMSD does not change significantly up to 1.8 ns after which it increases slightly and attains a value ~0.3 nm at 2.5 ns due to loss of C-terminal 3_{10} helix (residues 57–59). The RMSD remains the same till 5 ns and increases again until it reaches a value of 0.4 nm at 5.1 ns due to the loss of N-terminal 3_{10} helix (residues 19–21). At around 6.3 ns RMSD increases further and reaches a value of 0.45 nm due to transient disappearance of the α-helix (residues 37–40), after that RMSD decreases to a value of 0.3 nm at around 7 ns due to the reappearance of the α-helix. RMSD remains the same afterwards for rest of the simulation.

At 423 K RMSD increases sharply till 2.3 ns and reaches a value of 0.85 nm showing the triggering of the unfolding. Within this time the protein loses all the 3_{10} helices and C-terminal region gets highly distorted. At around 5 ns the protein loses the α-helical region (residues 37–40) and RMSD reaches a value ~1 nm. A plateau is obtained in the curve after 5 ns when rearrangement of β-strands occurs.

At 473 K RMSD attains a large value from the beginning of the simulation. Within 300 ps it reaches ~0.6 nm and at around 1.5 ns the protein loses all the secondary structure and becomes coiled. The maximum RMSD value at this temperature exceeds 1.4 nm.

3.1.2. Radius of gyration

The radius of gyration (Rg) is defined as the mass-weighted root mean square distance of a collection of atoms from their common center of mass. Hence, this analysis gives us insight into the overall dimensions of the protein. The plot of radius of gyration of the protein versus time at different temperatures is shown in Fig. 2b. At 277 K and 298 K simulations the Rg plots show similar trends. Two curves do not differ significantly and maintain the lowest value of Rg around ~1.05 nm, indicating that the compact conformation is largely preserved at these temperatures. At 373 K simulation, the Rg exhibits a jump from 1.05 nm to 1.15 nm at around 6 ns due to transient disappearance of the α-helix. Rg reaches a value of ~1.05 nm at around 7 ns when the reformation of the α-helix occurs. Rg remains the same afterwards for rest of the simulation.

At 423 K simulation a sharp increase of Rg is observed at around 2.3 ns when complete destruction of all 3_{10} helices and distortion of C-terminal region take place. After 5 ns Rg starts to rise again and reaches to a level of 1.2 nm at 6 ns. During this time the protein loses the α-helical region (residues 37–40). Afterwards Rg fluctuates roughly within 1.15 ± 0.15 nm mainly due to rearrangement of β-sheet region that differs from the initial conformation.

The curve corresponding to the 473 K simulation fluctuates more markedly. The maximum Rg value reaches at this temperature is ~1.5 nm. At 473 K there are three sudden jumps of Rg values around 2.5 ns, 5.5–6.5 ns, and 9 ns when Rg reaches the values of 1.3 nm, 1.5 nm and 1.45 nm, respectively. These are due to the complete loss of all the secondary structures.

3.1.3. SASA

The change of solvent accessible surface area (SASA) of the protein with time at different temperatures is shown in Fig. 2c. In all cases there is a systematic increase in SASA in the protein with the increasing temperature. Although the value of SASA increases

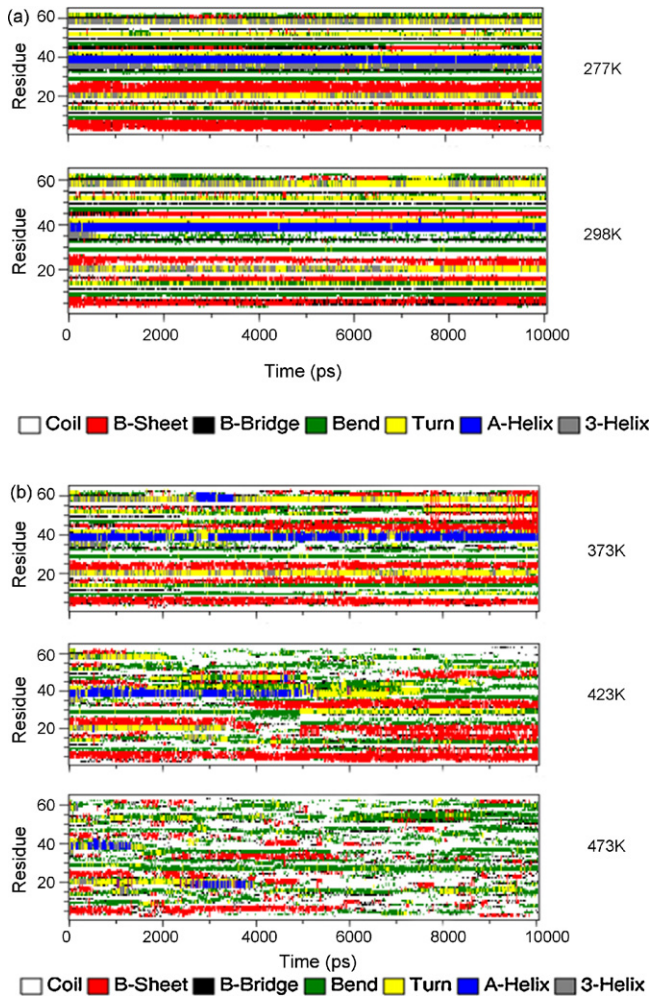

Fig. 3. Time evolution of the secondary structural elements of the protein at different temperatures (DSSP classification): (a) 277 K and 298 K; (b) 373 K, 423 K and 473 K.

with the increasing temperature but it remains essentially constant throughout the simulations at each temperature.

3.1.4. RMSF

A more detailed picture of differences in residue mobility within and between simulations can be obtained from graphs of the root mean-square fluctuations (RMSF) of C_α atoms relative to the average structure. Such fluctuations have been calculated for every temperature simulations. Fig. 2d shows the RMS fluctuations per residue over the production run (10 ns) of 277 K does not exceed 0.3 nm. The regions of greatest flexibility correspond to the termini of the protein and also in the loop region. The regular secondary structure regions show small fluctuations during the simulations. The RMSFs observed for 277 K, 298 K and 373 K simulations exhibit more or less similarly distributed fluctuations. However at 423 K and 473 K simulations most of the residues become highly mobile therefore the curve shows a lot more fluctuation. This is due to the loss of secondary structure at these high temperatures.

3.1.5. Secondary structure

Additional information on the structural flexibility of AFPIII is obtained by the analysis of time-dependent secondary structure fluctuations. Fig. 3a and b shows the secondary structural elements as a function of simulation time. Fig. 3a reveals that β-sheets, α-helices and 3_{10} helices observed within AFPIII crystal structure are maintained stably throughout the whole simulation period at 277 K. At 298 K the structure exhibits slight deviation from starting crystal structure. Only intermediate 3_{10} helix (residues 34–36) gets disrupted while rest two 3_{10} helices and α-helix are maintained throughout the simulation. The β-sheets of the starting structure alter between β-bridges and strands (Fig. 3a). At 373 K, all 3_{10} helices get completely denatured early in the simulation. Original β-strands of the crystal structure are not maintained and additional β-strands appear (Fig. 3b). At 423 K simulation all three 3_{10} helices are lost completely in the beginning of the simulation (within 2.3 ns). The C-terminal region of the protein becomes highly distorted due to the loss of C-terminal 3_{10} helix. α-Helix (residues 37–40) is maintained only for 5 ns. Rearrangements of secondary structural elements are observed toward the end of the simulation and additional β-sheets develop in the structure (Fig. 3b). At 473 K simulation, the 3_{10} helices exist only for a very few ps, the α-helix gets denatured within 1 ns. The structure becomes very disorganized with loss of almost all the secondary structure (Fig. 3b).

3.2. Intramolecular contacts

3.2.1. Hydrogen bonding pattern

The starting structure of AFPIII contains 43 intramolecular hydrogen bonds (shorter than 0.35 nm). The average numbers of hydrogen bonds are 41, 37, 33, 27, 23 for the 277 K, 298 K, 373 K, 423 K, 473 K simulations, respectively. Thus, as the simulation temperature is increased, there is a concomitant decrease in number of intact hydrogen bonds. This is reasonable as the structures become more distorted as the simulation temperature is raised. It is also evident from the plot (Fig. 4a) that although the number of hydrogen bonds varies in different temperature but it is steadily maintained throughout the simulations.

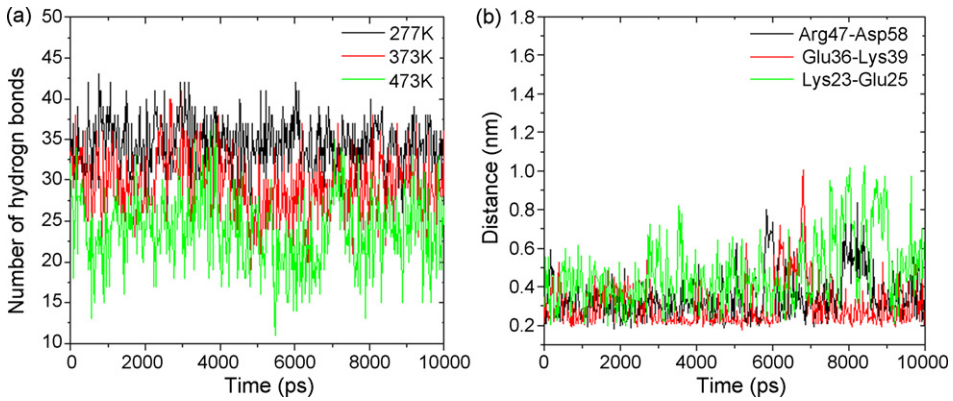

Fig. 4. Time evolution of (a) hydrogen bonds of the protein at three different temperatures and (b) three important ion pairs at 277 K.

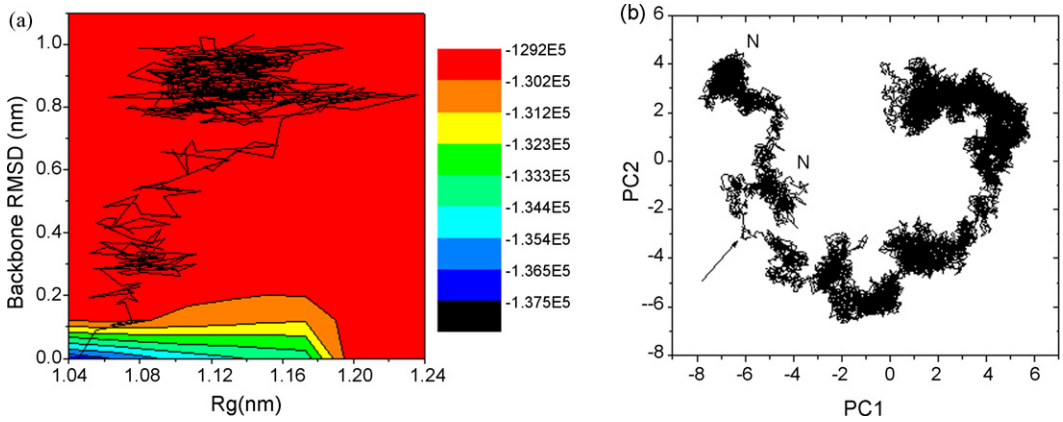

Fig. 5. (a) Potential energy contour plot of the protein where *X*-axis represents Rg and *Y*-axis represents backbone RMSD at 423 K. (b) Projection of the motion of the protein in phase space along the first two principal eigenvectors at 423 K. The clusters corresponding to the native state are marked with the letter N. An arrow indicates the region corresponding to the transition state.

3.2.2. Salt-bridge network

Salt bridges have shown to play an important role on the structural stability of AFPIIIs [1]. Three solvent exposed salt bridges (Glu36-Lys39, Arg47-Asp58, Lys23-Glu25) have been monitored throughout the simulations at five different temperatures. Fig. 4b shows the distances of the three salt bridges over time at 277 K. It is evident from the plot that Glu36-Lys39 salt bridge is only maintained throughout the simulation (within 0.6 nm) without any transient separation. In contrast, Lys23-Glu25 salt bridge is not maintained at all during the simulation. The Arg47-Asp58 salt bridge spends considerable time away from the short distances although the separations between the pairing residues are recovered during the simulation. These results suggest that the Glu36-Lys39 salt bridge may be more important for stability than the other two salt bridges. Our result is in agreement with previous experimental study where it has been shown that the Glu36-Lys39 salt bridge contributes significantly (∼1 kcal/mol) to AFPIIIs stabilization [1]. It is worth mentioning that none of these three salt bridges are maintained at 298 K or higher temperature simulations.

3.3. Ice-binding surface

AFPIII exhibits a flat ice-binding patch on its surface. Because the surface of ice crystal is macroscopically flat it binds to the ice by shape complementarities [20]. Eleven highly conserved ice-binding residues of this protein are Gln9, Leu10, Pro12, Ile13, Asn14, Thr15, Ala16, Thr18, Ile20, Met21 and Gln44, respectively [7]. Most of the residues are located within the loop region, except residues 20 and 21 that are part of N-terminal 3_{10} helix. Residues 11, 16, 44 exist as an isolated β-bridge. It has been found that at 277 K simulation the side chain O atoms of Gln9, Thr15 and Thr18, the N atoms of Gln 44 and the main chain O atom of Ala 16 form a flat surface (Figure not shown). These residues have shown previously to form hydrogen bond with ice water molecule [2,20]. It has also been found that this flat plane is surrounded by neighboring hydrophobic residues (Leu10, Pro12, Ile13, Ile20 and Met21). The flatness of the ice-binding surface has been started to disappear during the early stages of 298 K simulation and has not been reappeared later part of the simulation. This flatness is not maintained at all in higher temperature simulations.

3.4. Kinetics of unfolding

In order to gain insight about the kinetics of the system at different temperatures we monitor two different structural features (Rg and RMSD) and study how they vary concurrently over time. These quantities are plotted together, on the contour plot of the potential energy in Fig. 5a for 423 K simulation. Plots like these are generated for four other simulations (data not shown). These plots seem to have more of a diagonal movement in Rg and backbone RMSD space, which seem to show apparent two-state kinetics representing simultaneous collapse of the chain and the formation of denatured structure. The absence of many stable clusters throughout the pathway indicates that the protein unfolds without many detectable stable intermediates suggestive of two-state unfolding kinetics. This finding is in agreement with earlier thermodynamic study that suggests that the folding equilibrium of AFPIII is a two-state process with no populated intermediates [1]. The plot in Fig. 5a shows one large cluster at high values of Rg and backbone RMSD at the end point of the simulation. This expanded cluster spans from 2.9 ns to 10 ns simulation. The spread of the cluster indicates the heterogeneity of structures. Structures isolated from the middle of the cluster (around 5 ns) are devoid of α-helix (residues 37–40) whereas structures belonging towards the end of the cluster (8.5 ns) are mostly denatured without having α-helix or β-sheet. Some of these end point structures however possess rearranged β-strands that differ from the native one.

3.5. Identification of the transition state from projection

Essential dynamics is a method that utilizes principal component analysis (PCA) on the actual coordinates of the system and thus gives the essential motion of the protein in phase space [19]. Identification of transition state by this method is reliable because the important motion of the protein through phase space is considered [21]. The plot in Fig. 5b shows the motion of AFP in phase space during 423 K simulation projected along its first two principal components for atomic motion. The plot in Fig. 5b has two clusters corresponding to native states. The protein initially has passed through an expanded native-like conformation where no rapid conformational change occurred in them. A transiently populated area just after the native clusters corresponds to the transition state where initiation of rapid conformational changes occurs. Thus the transition states are identified as points just after population of the native state using the reasoning of Kazmirski et al. [22]. Kazmirski et al. define a region just before the first major structural change as the transition state. The reason behind this is that, for a process where the enthalpy increases and the entropy changes very little, a high free energy barrier is produced [22]. Two-transition state structures have been identified between 2.25 ns and 2.3 ns simulations. These structures are slightly different having close resemblance to the native secondary structures. However the one unifying feature is that they both are

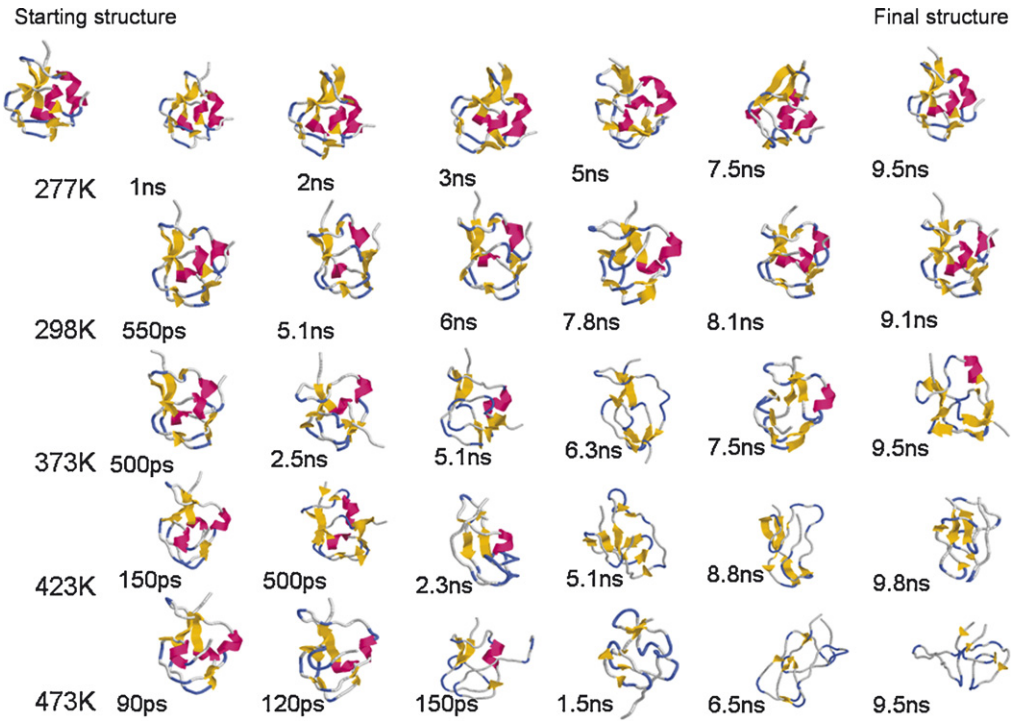

Fig. 6. Snapshots of the protein structure evolved at different time points at different temperatures. The structures having similar secondary structures but generated at different temperatures have been put in a same column. The first column shows initial disruption of the intermediate 3_{10} helix, followed by loss of C- and then N-terminal 3_{10} helices, fourth column shows loss of α-helix followed by rearrangement of β-strands.

devoid of 3_{10} helices (residues 19–21; residues 34–36; residues 57–59) and C-terminal regions are highly disrupted in them (Fig. 3b).

In summary two-transition state structures maintain native like helix and β-sheet but all have highly disrupted C-terminal. In this transition region the radius of gyration rises to levels reaching 1.2 nm before collapsing down to about basal level. RMSD rises up to 0.8 mn. This rise and fall of the radius and rise of RMSD are associated with the movement of the 3_{10} helices and the complete disruption of C-terminal region. Identification and analysis of the transition state are carried out for 473 K simulation where we have found that the transition state is present around 500 ps (figure not shown).

3.6. Unfolding pathway

Fig. 6 shows the snapshots of AFPIII during 10 ns MD simulations at different temperatures (277 K, 298 K, 373 K, 423 K and 473 K). It is obvious that the structure is uniformly stable at 277 K. At 298 K simulation the structural changes start to appear only after 500 ps when small 3_{10} helix (residues 34–36) starts to unfold. This is a result of the loss of the Glu 36:N-Pro 33:O hydrogen bond. The next structural change at 298 K occurs after 5 ns when C-terminal 3_{10} helix (residues 57–59) unfolds due to the loss of Met 59:N-Met 56 O and Val 60 N:Pro 57 O hydrogen bonds. This helix is however reformed again after 7.5 ns and remains stable during rest of the simulation. When the temperature is increased to 373 K, small 3_{10} helix (residues 34–36) disappears within 500 ps. At around 2.5 ns the C-terminal 3_{10} helix (residues 57–59) unfolds. The N-terminal 3_{10} helix (residues 19–21) unfolds after 5 ns. This is again a result of the losses of the Met 21:N-Thr 18:O and Met 22:N-Leu 19:O hydrogen bonds. At around 6 ns α-helix transiently disappears which however appears at around 7 ns. When the temperature is even raised to 423 K the protein unfolds rapidly. 3_{10} helix (residues 34–36) disappears at the very beginning of the simulation. Within 2.2–2.3 ns the C-terminal 3_{10} helix (residues 57–59) and other two 3_{10} helices (residues 19–21 and residues 34–36) unfold. (These events lead to a complete melting of the C-terminal.) The α-helical region (residues 37–40) disrupts after 5 ns. There has been a rearrangement of secondary structure especially in the β-sheet region after 6 ns as a result new β-sheets appear in the structure while original β-sheets are lost. The rearranged structure remains stable for the rest of the simulation. This is mostly due to the loss of Val 49:N-Ile 11:O; Val 49:O-Ile 11:N; Ser 4:N-Glu 25:O; Ser 4:O-Glu 25:N; Val 6:N-Lys 23:O; Val 6:O-Lys 23:N involving β-sheets. However, several new hydrogen bonds appear in the structure which include Thr 15:O-Val 49:N; Thr 15:N-Val 49:O; Val 6:N-Leu 19:O; Val 6:O-Leu 19:N; Ser 4:O-Met 21:N; Met 21:O-Ser 4:N; Asn 14:O-Ala 16:N; Gly 31:N-Met 59:O; Ile 20:N-Met 22:O. At 473 K simulation, the molecular contacts are lost much faster than at lower temperatures, for example the C- and N-terminal of AFPIII unfold within 150 ps. The α-helix remains stable up to 1 ns. After a short period of simulation (1.5 ns) the protein becomes highly distorted. The protein loses all the secondary structural elements and shows only a few β-bridges, the structure becomes almost coiled.

Comparative unfolding studies of psychrophilic and mesophilic uracil DNA glycosylase by molecular dynamics simulations have been reported previously at three different temperatures namely 375 K, 400 K and 425 K [23]. According to this study, the protein unfolding proceeds slowly in the 375 K simulations and the structural ensembles show less fluctuation when compared to 400 K and 425 K simulations. The unfolding rate is faster when the temperature is raised to 400 K. However, at 375 K and 400 K simulations psychrophilic enzyme shows higher level of unfolding compared to their mesophilic counterpart [23]. Destruction of the native protein structures occurs very fast when the temperature is raised to 425 K, and unfolding of psychrophilic and mesophilic enzymes proceeds at a similar rate [23].

In our simulation the lowest temperature at which unfolding events first observed is 373 K however the protein unfolding proceeds slowly at this temperature. The unfolding process

accelerates at 423 K simulation with the destruction of the native structure, which becomes even faster at 473 K simulation. To date there is no information regarding the structure of any AFPIII at very high temperature. Our study is the first attempt to observe the dynamic behavior of AFPIII at different temperatures.

4. Conclusion

The temperature-induced unfolding pathway of AFPIII is probed using molecular dynamics simulation. In our simulation the lowest temperature at which unfolding events first observed is 373 K however the protein unfolding proceeds slowly at this temperature. The unfolding process accelerates at 423 K simulation, which becomes even faster at 473 K simulation. It has been noted that similar unfolding events occur at the earlier time points as the temperature is increased. Thus increasing temperature accelerates protein unfolding without changing the pathway of unfolding. Trajectories in phase space give us insight into the two-state unfolding kinetics of this protein.

Our study provides insight into the structure–stability relationship of AFPIII, which may help to engineer AFPs with increased thermal stability that is more desirable than natural AFPs for some industrial and biomedical purposes.

Acknowledgements

This study was supported by grants from Department of Biotechnology, Govt. of India. We thank Dr. Chaitali Mukhopadhyay for her suggestions.

References

[1] O. Garcia-Arribas, R. Mateo, M.M. Tomczak, P.L. Davies, M.G. Mateu, Thermodynamic stability of a cold-adapted protein, type III antifreeze protein, and energetic contribution of salt bridges, Protein Sci. 16 (2007) 227–238.
[2] G. Chen, Z. Jia, Ice-binding surface of fish type III antifreeze, Biophys. J. 77 (1999) 1602–1608.
[3] M. Griffith, K.V. Ewart, Antifreeze proteins and their potential use in frozen foods, Biotechnol. Adv. 13 (1995) 375–402.
[4] G. Breton, J. Danyluk, F. Ouellet, F. Sarhan, Biotechnological applications of plant freezing associated proteins, Biotechnol. Annu. Rev. 6 (2000) 59–101.
[5] J. Kaiser, New prospects for putting organs on ice, Science 295 (2002) 1015.
[6] L.H. Wang, M.C. Wusteman, M. Smallwood, D.E. Preg, The stability during low-temperature storage of an antifreeze protein isolated from the roots of cold-acclimated carrots, Cryobiology 44 (2002) 307–310.
[7] T.P. Ko, H. Robinson, Y.G. Gao, C.H. Cheng, A.L. DeVries, A.H. Wang, The refined crystal structure of an eel pout type III antifreeze protein RD1 at 0.62-Å resolution reveals structural microheterogeneity of protein and salvation, Biophys. J. 84 (2003) 1228–1237.
[8] E. Lindahl, B. Hess, D. van der Spoel, Gromacs 3.0: a package for molecular simulation and trajectory analysis, J. Mol. Model. 7 (2001) 306–317.
[9] D. van der Spoel, E. Lindahl, B. Hess, G. Groenhof, A.E. Mark, H.J. Berendsen, GROMACS: fast, flexible, and free, J. Comput. Chem. 26 (2005) 1701–1718.
[10] W.F. van Gunsteren, S.R. Billeter, A.A. Eising, P.H. Hunenberger, P. Kruger, A.E. Mark, W.R.P. Scott, I.G. Tironi, Biomolecular Simulation: The Gromos 96 Manual and User Guide, Zurich, Switzerland: Hochschulverlag AG an der Zurich, 1996.
[11] H.J.C. Berendsen, J.P.M. Postma, W.F. van Gunsteren, J. Hermans, Interaction models for water in relation to protein hydration, in: B. Pullman (Ed.), Intermolecular Forces, D Reidel Publishing Company, Dordrecht, 1981 , pp. 331–342.
[12] H.J.C. Berendsen, J.P.M. Postma, A. DiNola, J.R. Hakk, Molecular dynamics with coupling to an external bath, J. Chem. Phys. 81 (1984) 3684–3690.
[13] B. Hess, H. Bekker, H.J.C. Berendsen, J.G.E.M. Fraaije, Lincs: a linear constraint solver for molecular simulations, J. Comput. Chem. 18 (1997) 1463–1472.
[14] T. Darden, D. York, L. Pedersen, Particle Mesh Ewald: an N-log (N) method for Ewald sums in large systems, J. Chem. Phys. 98 (1993) 10089–10093.
[15] U. Essmann, L. Perera, M.L. Berkowitz, T. Darden, H. Lee, L.G. Pederson, A smooth particle meshes Ewald potential, J. Chem. Phys. 103 (1995) 8577–8592.
[16] W. Kabsch, C. Sander, Dictionary of protein secondary structure: pattern recognition of hydrogen-bonded and geometrical features, Biopolymers 22 (1983) 2577–2637.
[17] D. van der Spoel, E. Lindahl, B. Hess, A.R. van Buuren, E. Apol, P.J. Meulenhoff, D.P. Tieleman, A.L.T.M. Sijbers, K.A. Feenstra, R. van Drunen, H.J.C. Berendsen, Gromacs User Manual Version 3.3, 2005, http:\\ww w.gromacs.org.
[18] R.A. Sayle, E.J. Millner-White, Rasmol-biomolecular graphics for all, Trends Biochem. Sci. 20 (1995) 374–376.
[19] A. Amadei, A.B. Linssen, H.J.C. Berendsen, Essential dynamics of proteins, Proteins 17 (1993) 412–425.
[20] Z. Jia, C.I. DeLuca, H. Chao, P.L. Davies, Structural basis for the binding of a globular antifreeze protein to ice, Nature 384 (1996) 285–286.
[21] N.J. Marianayagam, S.E. Jackson, The folding pathway of ubiquitin from all-atom molecular dynamics simulations, Biophys. Chem. 111 (2004) 159–171.
[22] S.L. Kazmirski, A. Li, V. Daggett, Analysis methods for comparison of multiple molecular dynamics trajectories: applications to protein unfolding pathways and denatured ensembles, J. Mol. Biol. 290 (1999) 283–304.
[23] M. Olufsen, B.O. Brandsdal, A.O. Smalås, Comparative unfolding studies of psychrophilic and mesophilic uracil DNA glycosylase: MD simulations show reduced thermal stability of the cold-adapted enzyme, J. Mol. Graph. Model. 26 (2007) 124–134.